The Palaeoproterozoic Francevillian succession of Gabon and the Lomagundi-Jatuli Event

Karen Bakakas[1], Mathieu Moussavou[1], Anthony R. Prave[2], Aivo Lepland[3,4], Michel Mbina[1], and Kalle Kirsimäe[4]

[1]Department of Geology, Université des Sciences et Techniques de Masuku, 943 Franceville, Gabon

[2]School of Earth and Environmental Sciences, St Andrews University, KY16 9AL St Andrews, Scotland

[3]Geological Survey of Norway, 7491 Trondheim, Norway

[4]Department of Geology, Tartu University, 50411 Tartu, Estonia

ABSTRACT

The Palaeoproterozoic Francevillian succession of Gabon has figured prominently in concepts about Earth's early oxygenation and genesis of a large positive excursion in C-isotope values, the Lomagundi-Jatuli event (LJE). Here we present a detailed study of a 139-m-long core of Francevillian rocks marked by $\delta^{13}C_{carb}$ values of 5 to 9‰ that decline up-section to near 0‰, a trend inferred by many workers as a fingerprint of the LJE and its termination. However, we show that the shift in C_{carb} values coincides with a facies change: shallow-marine facies are marked by the strongly positive values whereas deeper-marine facies (below storm wave base) are at ~0‰. The most circumspect interpretation of such facies dependence on $\delta^{13}C_{carb}$ is that shallow-marine settings record the isotope effects of local physical and biochemical processes driving the ambient dissolved inorganic carbon (DIC) pool to heavier values and the lighter values (~0‰) in deeper-water facies track the DIC of the open-marine realm where $\delta^{13}C$ was largely unaffected by fractionations occurring in shallow-water settings. Further, a transgressing redoxcline created conditions for precipitation of Mn-bearing minerals and chemotrophic microbial biota, including methane cycling communities evident by $\delta^{13}C_{org}$ values of -47‰ and $\Delta\delta_{carb-org}$ values as high as 46‰. Thus, the Francevillian C-isotope profile reflects basin-specific conditions and is not *a priori* an indicator of global C-cycle disturbances nor of the termination of the LJE.

INTRODUCTION

The first part of the Palaeoproterozoic Era (2.5 – 2.0 Ga) was marked by oxygenation of the atmosphere and loss of S-MIF (Great Oxidation Event of Holland, 2006; Farquhar et al., 2000), one of the largest ever positive excursions in carbonate $\delta^{13}C$ values (the Lomagundi-

Jatuli Event of Karhu and Holland, 1996) and deposition of exceptionally organic-rich rocks (Shunga Event; Melezhik et al., 1999). Understanding the genesis of these events requires identifying processes of cause-and-effect and attributing them correctly to those that are either bespoke to individual basin conditions or a consequence of wholesale Earth system change. Here we focus on the Lomagundi-Jatuli Event (LJE) that has been championed by many workers as a synchronous and global reorganisation of the C-cycle (Bekker et al., 2006; Maheshwari et al., 2010; Bekker and Holland, 2012); underpinning this interpretation is the observation that large, positive excursions in $\delta^{13}C_{carb}$ values are documented in rocks between 2.3 - 2.1 Ga in age on every continent except Antarctica (Martin et al., 2013; She et al., 2016). To assess the drivers of the LJE, we use new sedimentological, C-O isotope, geochemical and mineralogical data from a 139-m-long core of rocks of the Palaeoproterozoic Francevillian succession of Gabon that contain a C-isotopic trend attributed to the LJE (Préat et al., 2011; Canfield et al., 2013; Ossa Ossa et al., 2018).

GEOLOGICAL SETTING

The Palaeoproterozoic Francevillian basin in Gabon (Fig. 1) covers 42k km^2 and is divided into the Franceville, Okondja, Lastoursville and Booué sub-basins (Weber, 1968). It contains a mildly deformed (broad open folds cut by high angle faults) succession that is from several tens to many hundreds of metres thick (Thiéblemont et al., 2009). Five formations have been defined, from the base upward: FA - sandstone and minor conglomerate, FB - sandstone, black shale and dolostone, FC - dolostone, chert and jasper, FD - mostly black shale and FE - fine sandstone. U-Pb zircon ages of 2191±13 Ma for N'goutou Complex granite (Sawaki et al., 2017) that intrudes the lower part of the Francevillian succession in the Okondja sub-basin provides a minimum depositional age for the succession and 2083±6 Ma for a tuff in FD in the Lastoursville sub-basin (Horie et al., 2005) dates deposition of that Formation.

MATERIAL AND METHODS

Our observations and data come from outcrops and detailed sedimentary logging of core LST12 in the Lastoursville sub-basin (Fig. 2). LST12 recovered 139 m of dolostone and black shale that represent the FB-FC interval (Préat and Weber, 2019). 150 samples for geochemical and mineralogical analysis were taken between 17 to 139 m depths (Supplementary Information Tables S1-S4); above 17 m the core is weathered and was not sampled. Samples were analysed for petrography, major and minor elements, and mineral and stable isotope composition using analytical methods described in the Supplementary Information along with analytical data and supporting information.

CORE LST12

Six units comprise core LST12 (Units I-VI; Fig. 2). Units I and II, 12 and 17 m thick, respectively, are dark-grey dolostone and black shale; Unit I is dolostone dominated whereas Unit II has more shale interbeds. Sedimentary structures (Figs. 3A-B) include ripple cross-lamination, flaser bedding, mudstone drapes and reactivation surfaces and many ripples show bi-modal foresets (herringbone). Shales are marked by quartz, mica, K-feldspar, plagioclase and minor pyrite. In Unit I, dolomite content varies from a few percent in shale to c. 90% and scanning electron microscope (SEM) images show zonation caused by variable Fe substitution. In Unit II, dolomite content increases upward from c. 50 to 95% and is marked by massive aggregates with weak zonation under SEM (Fig. 3G).

Unit III is 46 m of pink-grey dolostone; the lower 36 m is cross-bedded dolostone interbedded with intraformational breccia and the upper 10 m is pink-grey dolomicrite with rhythmite-like layering. Sheet and desiccation cracks, herringbone cross-laminae and thin layers of crinkle-laminite are present. Pyrobitumen occurs as veins, fracture fills with calcite and silica, and reworked grains; the former occur in varying densities and as a fine mesh-like network in the dolomicrite interval (Fig. 3C). Dolomite makes up 60-80% of the mineral phases.

Unit IV is 11 m thick and consists of pyritiferous organic-rich black shale interspersed with 2-15 cm-thick beds of massive dark-grey to black dolostone with dispersed pyrite framboids (Fig. 3D). Shale is characterised by a quartz - K-mica assemblage and dolostone has zoned rhombs (Fig. 3H) with increasing Fe and Mn in outermost zones.

Unit V is 16 m thick, light- to dark-grey dolo-rhythmite and -laminite (Fig. 3E) interbedded with planar to low- angle dolostone, minor intraclastic beds and rare chert nodules. Dolomite content is 60-80% in the lower part decreasing to c. 45% in the upper part; silt-sized quartz and K-mica increase upward. Mn occurs as mixed-composition zoned Mn-Fe-Ca-carbonate in thin crusts or botryoidal-like nodules some of which have Mn-oxyhydroxides preserved in their cores.

Unit VI comprises the upper 23 m of the core (excluding the uppermost weathered portion) and is black shale (Fig. 3F) with minor thin beds of laminated to massive dolomicrite, siderite and siliceous dolomarl. Pyrite is abundant as nodules, disseminated grains and framboids. Mixed-composition zoned Mn-Fe-Ca-carbonate (Fig. 3I), similar to Unit V, is also present.

Lithofacies interpretation

Flaser bedding, reactivation surfaces, herringbone ripples and desiccation cracks in Units I-III indicate tidal and shallow-marine settings and dolo-breccias in Unit III are palaeokarst (Préat et al., 2011). The presence of pyrobitumen grains in Unit III attests to hydrocarbon migration and seeps being coeval with deposition. In contrast, rhythmite and laminite together with absence of ripples and cross bedding in Units IV-VI represent a deepening to depths below the influence of tide- and storm-generated currents. In summary, sedimentology shows Units I-III are tidal and shallow-marine deposits that experienced exposure and karsting and Units IV-VI record a transgression into bathymetries below effective storm wave base.

C-O isotopes: carbonate rocks and organic matter

$\delta^{13}C_{carb}$ values for the shallow-marine Units I-III range from 1.3 to 9.3‰ but are dominantly between 5 and 9‰ (Fig. 2) whereas deeper-marine Units IV-VI are marked by stepwise declines to lower values that stabilise around 0‰. The Mn-rich carbonates in the upper part of the core have large variability between -5 and -15‰. Organic matter from shallow-water Units I-III have $\delta^{13}C_{org}$ values from -25 to -30‰, deeper-water facies decline from c. -40‰ in Unit IV to c. -47‰ in Unit VI and values for pyrobitumen veins in Unit III are c. 15‰ lower than the carbonate host rocks but similar to Unit VI (Fig. 2). O isotopes are consistently between -5 and -10‰ through the entire profile.

Manganese abundances and mineralogy

The main carriers of Mn are Mn-Fe-Ca-carbonate phases. Mn concentrations are <0.1% in Units I-III, increase to 0.3% in Unit IV and reach >1% in Units V-VI. Mn/Ca ratios increase upward in Units IV-VI reflecting increasing abundance of Mn-carbonates relative to dolomite and coincides with negative shifts in both $\delta^{13}C_{carb}$ and $\delta^{13}C_{org}$ values.

DISCUSSION

Carbonate C-isotopes and implications for the LJE

Previous workers have advocated that the $\delta^{13}C_{carb}$ profile of the Francevillian rocks records the global termination of the LJE (Ossa Ossa et al., 2018). Our sedimentological data, however, show that C-isotope trends coincide with a change from shallow- to deeper-marine settings and confirm unambiguously that the decline in C-isotope values is directly concurrent with a deepening event, a coincidence not noted by previous workers. Isotope gradients from higher to lower $\delta^{13}C_{carb}$ values are known in modern and geologically recent settings from near surface seawater to coeval deeper pelagic settings, gradients that can be as much as 5‰ (Stiller et al., 1985; Sharp, 2007; Swart 2008; Swart and Eberli, 2005). For example, higher $\delta^{13}C_{carb}$ values in shallow settings can be explained as a consequence of evaporation and development of ^{13}C-enriched residual brines (Stiller et al., 1985) and by diurnal cycling between photosynthesis and associated carbonate precipitation in shallow seas with high bioproductivity (Geyman and Maloof, 2019). A C-isotope depth gradient in the Palaeoproterozoic is, therefore, not unexpected. For rocks this old, diagenetic resetting and overprinting is always a concern but our careful isotope and petrographic analyses show there is no evidence for such effects (see Supplementary Information for additional discussion on diagenesis). Therefore, the most objective interpretation of the $\delta^{13}C_{carb}$ isotope trend in core LST12 and correlative Francevillian sections (e.g. Ossa Ossa et al., 2018) is that they are due to basinal conditions, hence are not evidence of the end of LJE.

Manganese enrichment: a transgressing redoxcline

We interpret enrichment in Mn in Units IV-VI as having formed at a redoxcline (Roy, 2006) between upwelling anoxic deep waters containing dissolved Mn(II) and overlying oxic water masses (Fig. 4). This resulted in accumulation of Mn(IV)-oxyhydroxide precipitates at the seafloor that were subsequently reductively dissolved and reprecipitated as Mn-carbonates due to elevated pore water alkalinity from mineralisation of organic matter, analogous to Mn-carbonate formation from fluctuating redoxclines in the Baltic Sea (Sternbeck and Sohlenius, 1997). This is indicated by the strongly negative $\delta^{13}C_{carb}$ values of Mn-rich carbonate beds in Unit VI. Given the high TOC abundances (2-15%) in the Mn-rich intervals, it is likely that the upwelling water masses were also rich in nutrients thereby triggering high productivity at or above the redoxcline.

Distribution and isotopic composition of organic matter

The range of $\delta^{13}C_{org}$ values from -26 to -47‰ (Fig. 2) requires different carbon sources and metabolisms, not solely shallow- versus deeper-water settings (2-3‰ in modern seas; Hayes et al., 1999; Hayes and Waldbauer, 2006). Methanotrophic microbes produce biomass with $\delta^{13}C_{org}$ values <-37‰ (Eigenbrode et al., 2008) whereas values of -25 to -30‰ typify CO_2-utilising autotrophic organisms (Zerkle et al., 2005). The shift in $\delta^{13}C_{org}$ values, from -30 ±4‰ in Units I-III to 43 ±4‰, and as low as -47‰ (Fig. 2), through Units IV-VI along with $\Delta\delta_{carb-org}$ values as high as 46‰ in Units V-VI, coincides with transgression and appearance of Mn-rich carbonates. Thus, our data are best explained as recording a fluctuating redoxcline, high productivity and methanotrophy, the latter likely driven by microbial methane produced in the organic-rich sediment column (Boetius et al., 2000; Hattori, 2008). This implies that the Francevillian basin had a sharply redox-stratified water-column with photoautotrophs in oxygenated settings above, and heterotrophs and chemoautotrophs below the redoxcline.

CONCLUSION

Our integrated sedimentological and chemostratigraphic dataset shows that downturns in $\delta^{13}C_{carb}$ values, from consistently between 5-9‰ to near 0‰, and $\delta^{13}C_{org}$, from -26‰ to as low as -47‰, coincide with facies changes from shallow- to deeper-marine settings. We propose the former represents carbon isotope fractionation in shallow water settings as a consequence of enhanced bioproductivity and/or evaporation that drove precipitation of isotopically heavy carbonates and that coeval deeper-water settings record precipitation of carbonate from a pool marked by isotopically normal values (~0‰). The $\delta^{13}C_{org}$ trend reflects a stratified water column where an oxic/anoxic redoxcline formed in water depths that were below storm wave base; interactions between oxic surface waters and anoxic deeper waters along the redoxcline generated conditions for precipitation of Mn-oxyhydroxides and later alteration to Mn carbonates, and high organic productivity. The low $\delta^{13}C_{org}$ values indicate that deeper waters were dominated by chemotrophic consortia including methane cycling communities. The most circumspect interpretation of the Francevillian C-isotope profile is that it records conditions bespoke to its basinal setting: the positive C-isotope ‘event’ was confined to shallow-water platform settings whereas the $\delta^{13}C$ of open deep water DIC remained near 0‰. Our findings show the necessity for establishing robust sedimentological context for understanding Palaeoproterozoic C-isotope trends and basin specific processes before presuming an origin attributable to a global reorganisation of the C cycle.

ACKNOWLEDGEMENTS

Samples were provided by the Comilog-Eramet in Moanda, Gabon. We thank Alain Préat, Francis Wéber and Florent Pambo for discussion. Alexis Ndongo and Cédric Ligna provided assistance for the sampling of LST 12 core. Albertus Smith, Juha Karhu, Peter Swart and an anonymous reviewer are thanked for their constructive and most helpful criticism. The study was supported from Estonian Research Agency grant PRG447 to KK, AL and KB.

APPENDIX 1 – Supplementary Information

APPENDIX 2 – Supplementary Tables

REFERENCES CITED

Bekker, A., and Holland, H. D., 2012, Oxygen overshoot and recovery during the early Paleoproterozoic: Earth and Planetary Science Letters, v. 317, p. 295-304.

Bekker, A., Karhu, J. A., and Kaufman, A. J., 2006, Carbon isotope record for the onset of the Lomagundi carbon isotope excursion in the Great Lakes area, North America: Precambrian Research, v. 148, no. 1-2, p. 145-180.

Boetius, A., Ravenschlag, K., Schubert, C. J., Rickert, D., Widdel, F., Gieseke, A., Amann, R., Jorgensen, B. B., Witte, U., and Pfannkuche, O., 2000, A marine microbial consortium apparently mediating anaerobic oxidation of methane: Nature, v. 407, no. 6804, p. 623-626.

Canfield, D. E., Ngombi-Pemba, L., Hammarlund, E. U., Bengtson, S., Chaussidon, M., Gauthier-Lafaye, F., Meunier, A., Riboulleau, A., Rollion-Bard, C., Rouxel, O., Asael, D., Pierson-Wickmann, A. C., and El Albani, A., 2013, Oxygen dynamics in the aftermath of the Great Oxidation of Earth's atmosphere: Proceedings of the National Academy of Sciences of the United States of America, v. 110, no. 42, p. 16736-16741.

Eigenbrode, J. L., Freeman, K. H., and Summons, R. E., 2008, Methylhopane biomarker hydrocarbons in Hamersley Province sediments provide evidence for Neoarchean aerobiosis: Earth and Planetary Science Letters, v. 273, no. 3-4, p. 323-331.

Farquhar, J., Bao, H., and Thiemens, M., 2000, Earth’s earliest sulfur cycle: Science, v. 289, p. 756-758.

Geyman, E.C. and Maloof, A.C., 2019, A diurnal carbon engine explains ^{13}C-enriched carbonates without increasing the global production of oxygen: Proceedings of National Academy of Sciences of the United States of America, v. 116, p. 24433-24439.

Hattori, S., 2008, Syntrophic acetate-oxidizing microbes in methanogenic environments: Microbes and Environments, v. 23, no. 2, p. 118-127.

Hayes, J. M., Strauss, H., and Kaufman, A. J., 1999, The abundance of C-13 in marine organic matter and isotopic fractionation in the global biogeochemical cycle of carbon during the past 800 Ma: Chemical Geology, v. 161, no. 1-3, p. 103-125.

Hayes, J. M., and Waldbauer, J. R., 2006, The carbon cycle and associated redox processes through time: Philosophical Transactions of the Royal Society B-Biological Sciences, v. 361, no. 1470, p. 931-950.

Holland, H. D., 2006, The oxygenation of the atmosphere and oceans: Philosophical Transactions of the Royal Society B-Biological Sciences, v. 361, no. 1470, p. 903-915.

Horie, K., Hidaka, H., and Gauthier-LaFaye, F., 2005, U-Pb geochronology and geochemistry of zircon from the Franceville series at Bidoudouma, Gabon: Geochimica et Cosmochimica Acta, v. 69, no. 10, p. A11-A11.

Karhu, J. A., and Holland, H. D., 1996, Carbon isotopes and the rise of atmospheric oxygen: Geology, v. 24, no. 10, p. 867-870.

Maheshwari, A., Sial, A. N., Gaucher, C., Bossi, J., Bekker, A., Ferreira, V. P., and Romano, A. W., 2010, Global nature of the Paleoproterozoic Lomagundi carbon isotope excursion A review of occurrences in Brazil, India, and Uruguay: Precambrian Research, v. 182, no. 4, p. 274-299.

Martin, A. P., Condon, D. J., Prave, A. R., and Lepland, A., 2013, A review of temporal constraints for the Palaeoproterozoic large, positive carbonate carbon isotope excursion (the Lomagundi-Jatuli Event): Earth-Science Reviews, v. 127, p. 242-261.

Melezhik, V. A., Fallick, A. E., Filippov, M. M., and Larsen, O., 1999, Karelian shungite - an indication of 2.0-Ga-old metamorphosed oil-shale and generation of petroleum: geology, lithology and geochemistry: Earth-Science Reviews, v. 47, no. 1-2, p. 1-40.

Ossa Ossa, F. O., Eickmann, B., Hofmann, A., Planavsky, N. J., Asael, D., Pambo, F., and Bekker, A., 2018, Two-step deoxygenation at the end of the Paleoproterozoic Lomagundi Event: Earth and Planetary Science Letters, v. 486, p. 70-83.

Preat, A., Bouton, P., Thieblemont, D., Prian, J. P., Ndounze, S. S., and Delpomdor, F., 2011, Paleoproterozoic high delta C-13 dolomites from the Lastoursville and Franceville basins (SE Gabon): Stratigraphic and synsedimentary subsidence implications: Precambrian Research, v. 189, no. 1-2, p. 212-228.

Preat, A., and Weber, F., 2019, Comment on Ossa Ossa et al. (2018) paper published in EPSL: Earth and Planetary Science Letters, v. 511, p. 256-258.

Roy, S., 2006, Sedimentary manganese metallogenesis in response to the evolution of the Earth system: Earth-Science Reviews, v. 77, no. 4, p. 273-305.

Sawaki, Y., Moussavou, M., Sato, T., Suzuki, K., Ligna, C., Asanuma, H., Sakata, S., Obayashi, H., Hirata, T., and Edou-Minko, A., 2017, Chronological constraints on the Paleoproterozoic Francevillian Group in Gabon: Geoscience Frontiers, v. 8, no. 2, p. 397-407.

Sharp, Z., 2007, Stable isotope geochemistry, Upper Saddler River, N.J, Pearson Education.

She, Z. B., Yang, F. Y., Liu, W., Xie, L. H., Wan, Y. S., Li, C., and Papineau, D., 2016, The termination and aftermath of the Lomagundi-Jatuli carbon isotope excursions in the Paleoproterozoic Hutuo Group, North China: Journal of Earth Science, v. 27, no. 2, p. 297-316.

Sternbeck, J. and Sohlenius, G., 1997, Authigenic sulfide and car-bonate mineral formation in Holocene sediments of theBaltic Sea: Chemical Geolgy, v. 135, p. 55-73.

Stiller, M., Rounick, J. S., and Shasha, S., 1985, Extreme carbon-isotope enrichments in evaporating brines: Nature, v. 316, no. 6027, p. 434-435.

Swart, P.K., 2008, Global synchronous changes in the carbon isotopic composition of carbonate sediments unrelated to changes in the global carbon cycle: Proceedings of National Academy of Sciences of the United States of America, v. 105, p. 13741-13745.

Swart, P. K., and Eberli, G., 2005, The nature of the delta C-13 of periplatform sediments: Implications for stratigraphy and the global carbon cycle: Sedimentary Geology, v. 175, no. 1-4, p. 115-129.

Zerkle, A. L., House, C. H., and Brantley, S. L., 2005, Biogeochemical signatures through time as inferred from whole microbial genomes: American Journal of Science, v. 305, no. 6-8, p. 467-502.

Thiéblemont, P., Castaing, C., Billa, M., Bouton, P., and Préat, A., 2009, Notice explicative de la carte géologique et des ressources minérales de la République Gabonaise à 1/1000 000: Libreville, Gabon: Ministère des Mines, du Pétrole, des Hydrocarbures.

Weber, F., 1968, Une série précambrienne du Gabon: le Francevillien Sédimentologie, géochimie, relations avec les gîtes minéraux associés: Université de Strasbourg, CEA-R-40055.

FIGURES

Figure 1. Francevillian succession of Gabon and simplified geological map of the Lastoursville sub-basin (after Thiéblemont et al., 2009). Sub-basins: B – Booue, F – Franceville, L – Lastoursville, O – Okondja.

Figure 2. Stratigraphy, C-O isotopes and Mn trends in core LST12. See Figure 1 for location and text for discussion.

Figure 3. Characteristic rock types and selected SEM images of LST12. A. Unit I (138 m core depth) dolostone interbedded with dark-grey to black shale with wavy lamination, ripple cross-lamination with mudstone drapes. B. Unit II (113 m core depth) dark- to tan-grey dolostone with parallel lamination and herringbone cross-bedding. C. Unit III (73 m core depth) grey to pink dolostone in part brecciated with pyrobitumen veinlets and fractures. D. Unit IV (60 m core depth) pyritiferous black shale and dark-grey dolomicrite with dispersed pyrite. E. Unit V (42 m core depth) light- to dark-grey/black Mn-rich dolo-rhythmite. F. Unit VI (27 m core depth) black shale with abundant pyrite and thin beds of Mn-rich dolomicrite. G-I. Backscattered electron mode SEM images; Dol – dolomite, Mic – mica, Py – pyrite, Q – quartz, Kf – K-feldspar, Sid – siderite: G - Unit I carbonate-mudstone contact marked by euhedral-subhedral rhombic dolomite crystals and silt and fine sand-sized quartz and feldspar in mica matrix with disseminated pyrite (127.8 m core depth); H - Unit IV dolomite bed composed of euhedral planar dolomite crystals with Fe- and Mn-rich outer rims (55.5 m core depth); I – Unit VI dolomite crystals with distinct Mn(Fe)-carbonate cores and Mn-rich siderite crystals (27.5 m core depth).

Figure 4. Depositional model of the Francevillian succession in LST12. Shallow-water carbonate rocks (Units I-III) are marked by enhanced productivity in the photic zone driving ^{13}C-enrichment in ambient DIC pool and depositing carbonates. Transgression ensues (Units IV-VI) with basin deepening marked by precipitation of isotopically normal marine carbonates concomitant with Mn enrichment at a redoxcline at depths that were below storm-wave base. Continued transgression results in deposition in deepest parts of the basin of organic-rich mudstones containing a methanotrophic biomass.

Figure 1

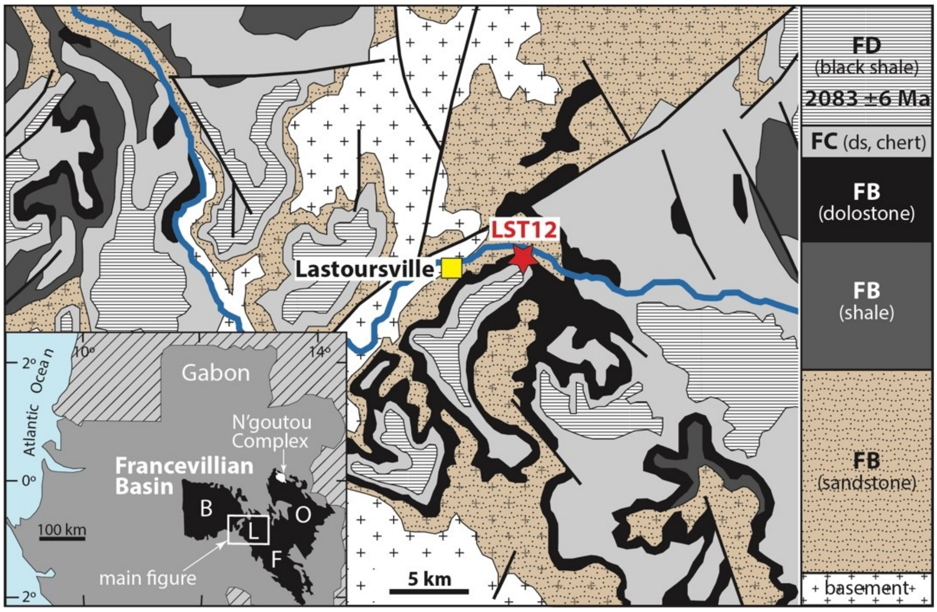
FD
(black shale)
2083 ±6 Ma
FC (ds, chert)
FB
(dolostone)
FB
(shale)
FB
(sandstone)
basement
LST12
Lastoursville
5 km
Gabon
Atlantic Ocean
N'goutou Complex
Francevillian Basin
B
L
O
F
100 km
main figure
10°
14°
2°
0°
-2°

Figure 2

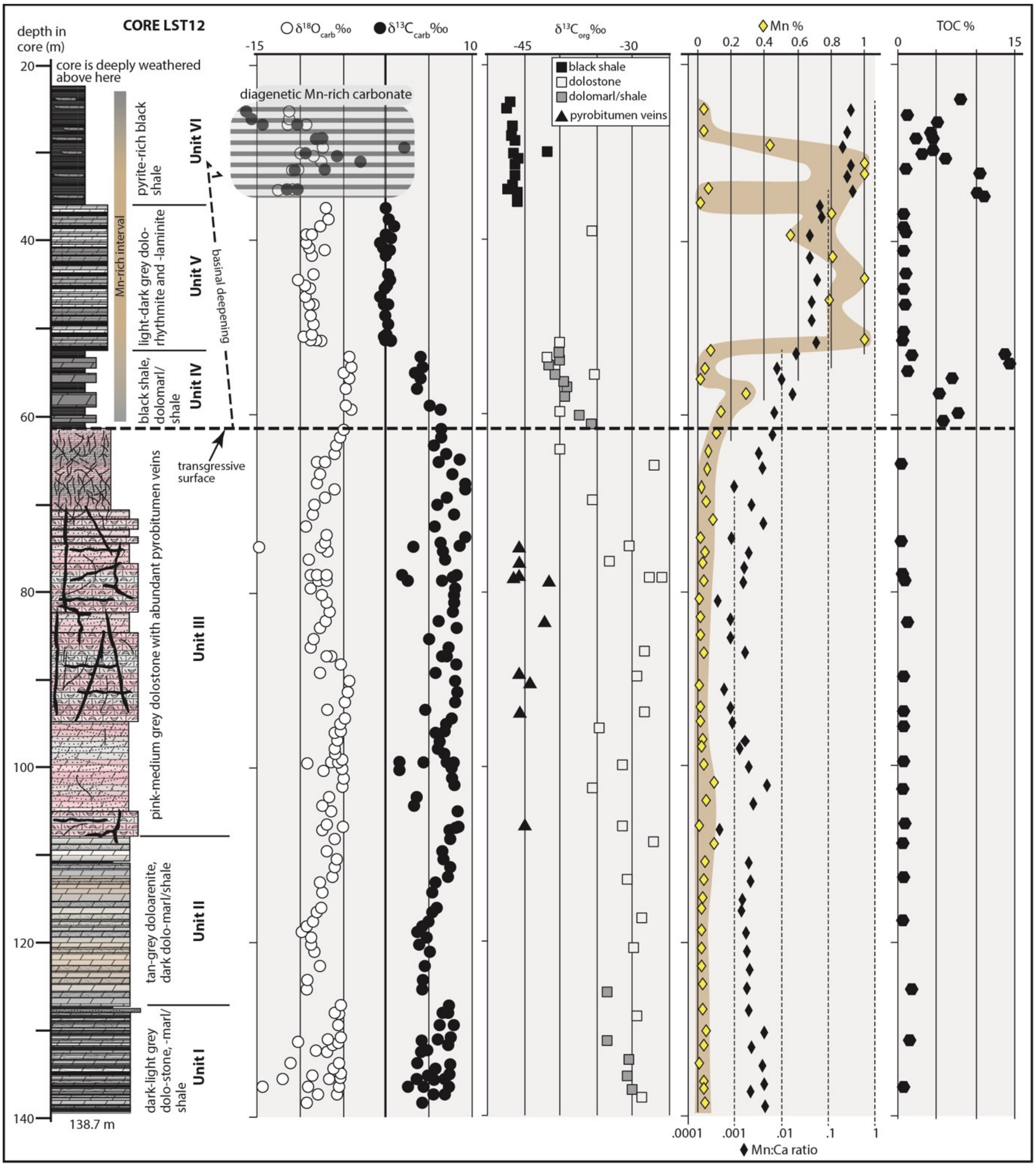
depth in core (m)
CORE LST12
core is deeply weathered above here
Mn-rich interval
pyrite-rich black shale
Unit VI
light-dark grey dolo-rhythmite and -laminite
Unit V
black shale, dolomarl/shale
Unit IV
basinal deepening
transgressive surface
pink-medium grey dolostone with abundant pyrobitumen veins
Unit III
tan-grey doloarenite, dark dolo-marl/shale
Unit II
dark-light grey dolo-stone, -marl/shale
Unit I
138.7 m
δ18Ocarb‰
δ13Ccarb‰
diagenetic Mn-rich carbonate
δ13Corg‰
black shale
dolostone
dolomarl/shale
pyrobitumen veins
Mn %
Mn:Ca ratio
TOC %

335 Figure 3

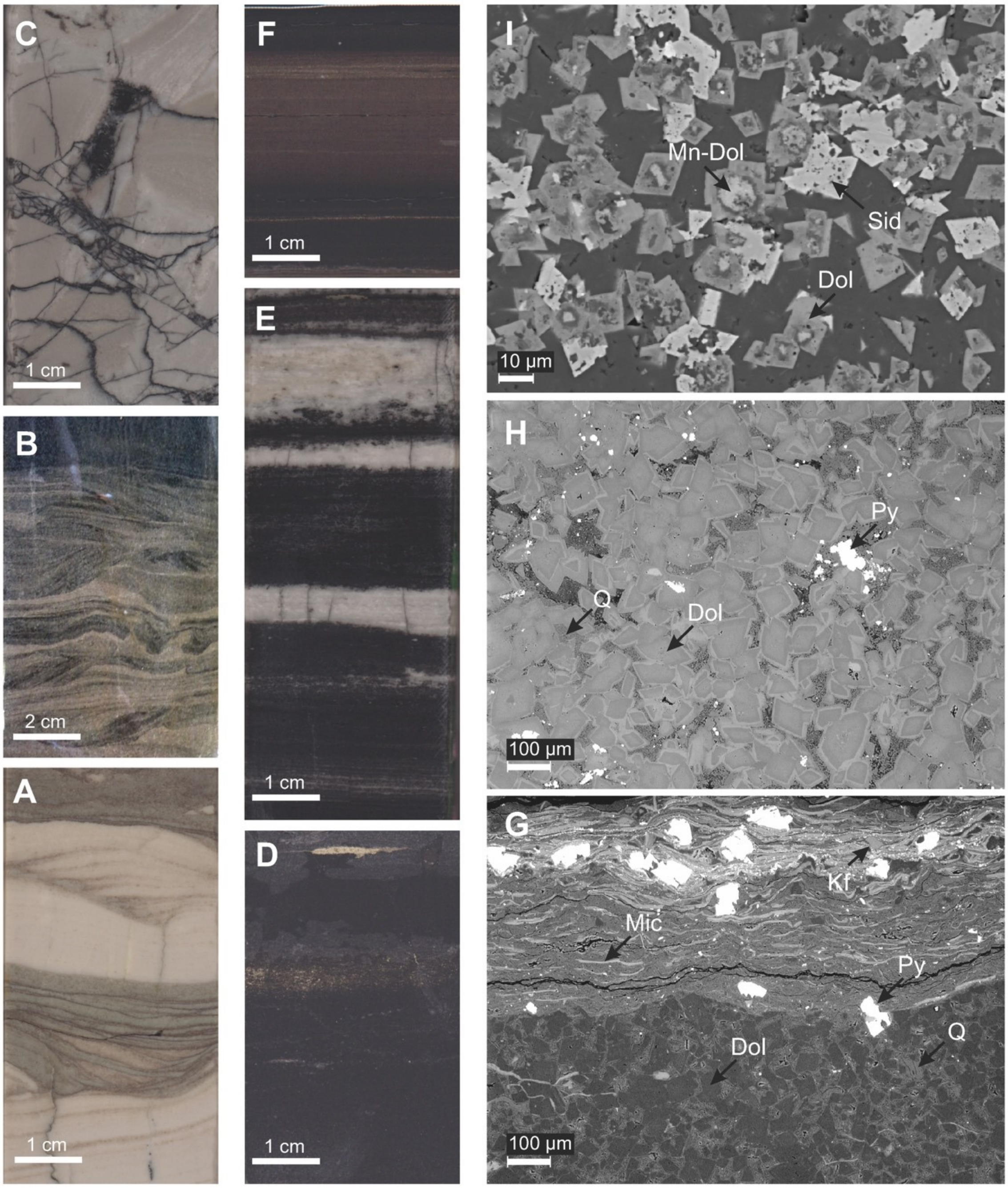

336

Figure 4

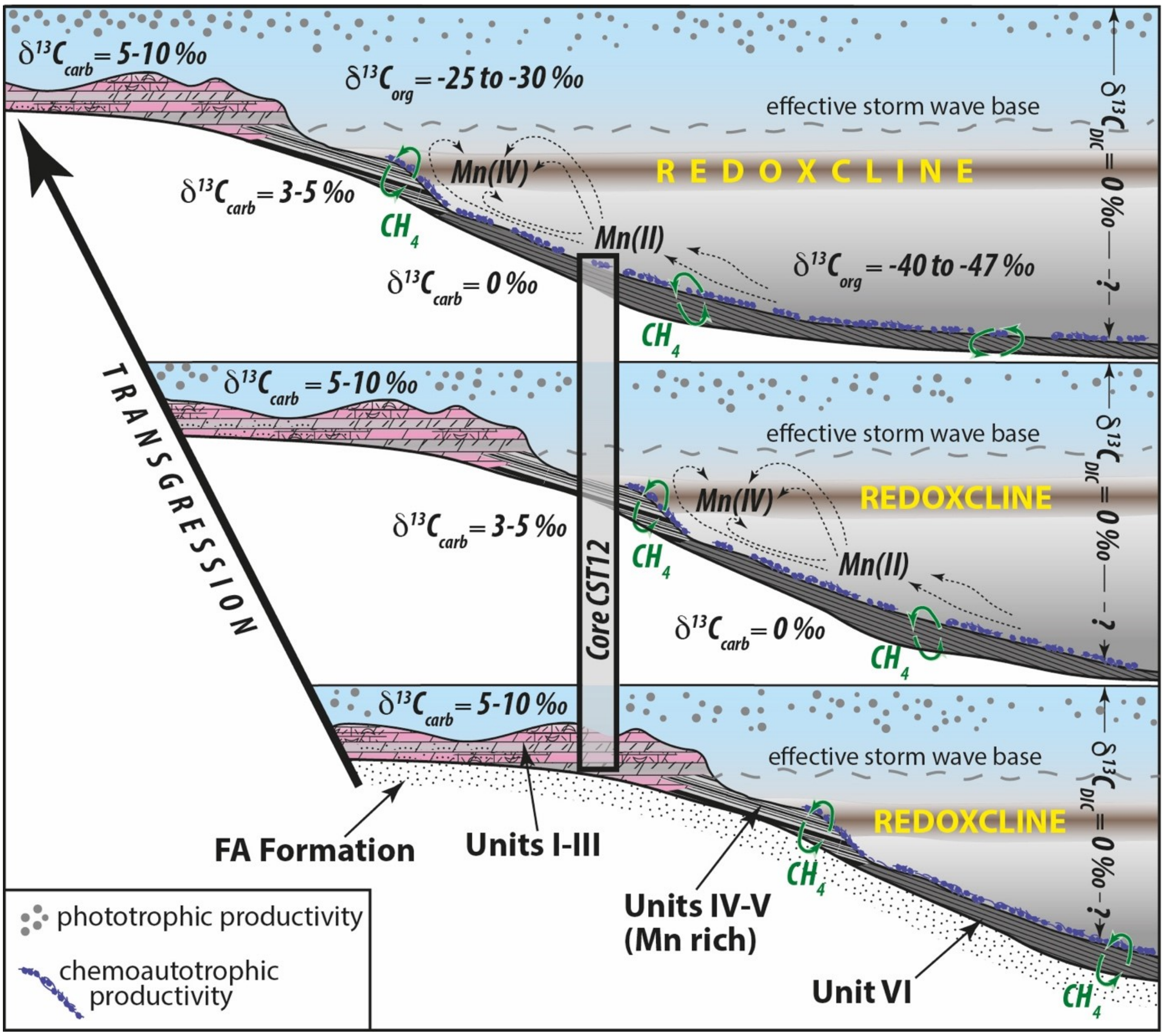

δ13Ccarb = 5-10 ‰
δ13Corg = -25 to -30 ‰
effective storm wave base
REDOXCLINE
Mn(IV)
δ13Ccarb = 3-5 ‰
CH4
Mn(II)
δ13Ccarb = 0 ‰
δ13Corg = -40 to -47 ‰
δ13CDIC = 0 ‰ — ?
TRANSGRESSION
Core CST12
FA Formation
Units I-III
Units IV-V
(Mn rich)
Unit VI
phototrophic productivity
chemoautotrophic productivity